

High-temperature dielectric response in pulsed laser deposited $\text{Bi}_{1.5}\text{Zn}_{1.0}\text{Nb}_{1.5}\text{O}_7$ thin films

Jitendra Singh,¹ A. T. Kalghatgi,¹ Jayanta Parui,² and S. B. Krupanidhi^{2,a)}

¹Central Research Laboratory, Bharat Electronics, Bangalore 560013, India

²Materials Research Centre, Indian Institute of Science, Bangalore 560012, India

(Received 28 April 2010; accepted 29 May 2010; published online 8 September 2010)

Cubic pyrochlore $\text{Bi}_{1.5}\text{Zn}_{1.0}\text{Nb}_{1.5}\text{O}_7$ thin films were deposited by pulsed laser ablation on Pt(200)/ SiO_2 /Si at 500, 550, 600, and 650 °C. The thin films with (222) preferred orientation were found to grow at 650 °C with better crystallinity which was established by the lowest full-width half maxima of ~ 0.38 . The dielectric response of the thin films grown at 650 °C have been characterized within a temperature range of 270–650 K and a frequency window of 0.1–100 kHz. The dielectric dispersion in the thin films shows a Maxwell–Wagner type relaxation with two different kinds of response confirmed by temperature dependent Nyquist plots. The ac conduction of the films showed a varied behavior in two different frequency regions. The power law exponent values of more than 1 at high frequency are explained by a jump-relaxation-model. The possibility of grain boundary related large polaronic hopping, due to two different power law exponents and transformation of double to single response in Nyquist plots at high temperature, has been excluded. The “attempt jump frequency” obtained from temperature dependent tangent loss and real part of dielectric constants, has been found to lie in the range of their lattice vibronic frequencies (10^{12} – 10^{13} Hz). The activation energy arising from a large polaronic hopping due to trapped charge at low frequency region has been calculated from the ac conduction behavior. The range of activation energies (0.26–0.59 eV) suggests that the polaronic hopping at low frequency is mostly due to oxygen vacancies. © 2010 American Institute of Physics. [doi:10.1063/1.3457335]

I. INTRODUCTION

Electrically tunable materials received more attention recently due to the rapidly increasing demands in wireless microwave communication applications, such as phase shifters and tunable antennas. For a microwave engineer, the ideal tunable material should combine a high tunability with low dielectric loss. Recently, cubic pyrochlore phase $\text{Bi}_{1.5}\text{Zn}_{1.0}\text{Nb}_{1.5}\text{O}_7$ (BZN) attracted much attention as a dielectric material for microwave tunable application mainly due to its very low dielectric loss.^{1,2} In addition, parallel-plate varactors employing C-BZN thin films demonstrated relatively higher total device quality factor of more than 200 up to 20 GHz, indicating a prospective application in microwave devices.²

Pulsed laser deposition (PLD) has merit in excellent control of the stoichiometric composition of complex oxide thin films, especially for BZN thin films due to the high volatility of Zn and Bi in case of radio frequency magnetron sputtering.^{3,4} As composition is the key factor to determine crystal structure and dielectric properties of BZN thin films,^{5,6} PLD technique is more practical to control the desirable cubic pyrochlore structure of BZN thin films. In this article, PLD technique has been applied to prepare the C-BZN thin films to grow at different temperatures for better crystallinity as well as better stoichiometry. Due to the dependence on stoichiometry, bismuth zinc niobate is tends to have two different structures: a cubic pyrochlore based on the BZN (C-BZN) composition and a monoclinic zirconolite

based on the $\text{Bi}_2\text{Zn}_{2/3}\text{Nb}_{4/3}\text{O}_7$ (*m*-BZN) composition, both compounds can be generally written as $(\text{Bi}_{3x}\text{Zn}_{2-3x}) \times (\text{Zn}_x\text{Nb}_{2-x})\text{O}_7$ with $x=0.5$ (cubic) and $x=2/3$ (monoclinic), respectively.^{7,8} However, the $\text{A}_2\text{B}_2\text{O}_7$ pyrochlore structure is often described by the formula $\text{B}_2\text{O}_6 \cdot \text{A}_2\text{O}'$, which suggests that the structure is built of two interpenetrating lattices with BO_6 octahedra sharing vertices form a three-dimensional network and thus results in large cavities which contain the O' and A atoms in an $\text{A}_2\text{O}'$ tetrahedral net.⁹ It was reported that A-site cations are randomly displaced by ~ 0.39 Å from the ideal eightfold coordinated positions in the lattice and the displacement occurs along the six $\langle 112 \rangle$ directions perpendicular to the O' –A– O' links along with a random displacement of the O' ions by 0.46 Å along all twelve $\langle 110 \rangle$ directions.^{7,10} However, it has been reported that in BZN (C-BZN), the possibility of A-site sharing by Bi^{3+} and Zn^{2+} can lead to a displacive disorder in O' –A– O' network which eventually reveals a lowest frequency vibrational bending mode resulting in high dielectric constant and dielectric relaxations.⁷ Though there are many reports on dielectric response of C-BZN in low temperature and high frequency, the dielectric studies at high temperature (above room temperature) are yet to be explored in detail. In the present paper, the dielectric response of BZN (C-BZN) has been reported within a temperature range of 270–650 K with a frequency window of 0.1–100 kHz in terms of dielectric dispersion, ac conductivity, attempt jump frequency, and polaronic hopping.

^{a)}Electronic mail: sbk@mrc.iisc.ernet.in

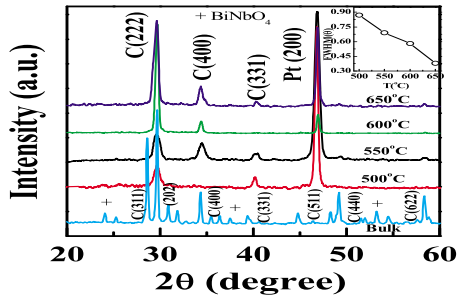


FIG. 1. (Color online) Room temperature XRD of BZN thin films deposited at 500, 550, 600, and 650 °C along with the XRD of bulk laser target. (inset) The FWHM of C(222) peaks obtained at different temperatures. (C stands for cubic pyrochlore).

II. EXPERIMENTAL PROCEDURE

The stoichiometric target of cubic pyrochlore C-BZN ceramics was prepared using the conventional solid reaction process. Bi_2O_3 , ZnO, and Nb_2O_5 powders were weighed according to the stoichiometric mole ratio of BZN, ball milled for 24 h, and then calcined at 800 °C for 4 h; 2 wt % organic binder was added to the powder to assist in forming. The calcined powders were pressed at 100 kN/cm² into a 15 mm diameter disk-shaped pellet and the pellets were sintered at 950 °C for 4 h. The C-BZN thin films were deposited on Pt(200)/SiO₂/Si substrates by PLD technique. A KrF excimer laser (Lambda Physik, Germany, 248 nm) was operated at a laser repetition frequency of 5 Hz. The substrate temperature during the deposition was maintained at 650 °C, with the laser fluence maintained at 1.5 J/cm² and substrate-target distance at 52 mm. The base pressure was initially brought down to 1.0×10^{-6} Torr and prior to the deposition, high-purity oxygen gas was introduced into the chamber and the deposition were carried at 50–200 mTorr. The phase composition and crystallization of the BZN thin films were analyzed by Bruker D8 Advance diffractometer (Cu $K\alpha$ $\lambda = 0.15418$ nm). The cross sectional scanning electron micrograph (SEM) was analyzed using scanning electron microscope (FEI XL40 Sirion FEG microscope). Circular gold dots of 300 μm diameter were deposited by thermal evaporation for the top electrodes (Au/BZN/Pt configuration). The electrode annealing was carried out at 325 °C for 15 min and the metal–insulator–metal (MIM) capacitor was used for the electrical characterization. Dielectric measurements were done using a programmable Keithley LCZ 3330 m (frequencies ranging from 0.1 to 100 kHz at oscillating amplitude of 500 mV). All the measurements on MIM capacitors were carried out at temperatures ranging between 270 to 650 K.

III. RESULTS AND DISCUSSION

A. Structural characterization

Figure 1 shows the x-ray diffraction (XRD) of bulk BZN and its thin films deposited on a Pt(200)/SiO₂/Si substrate within a temperature range from 500 to 650 °C. The oxygen partial pressure for the deposition has been kept at 100 mTorr for all the films. This diffraction pattern has been indexed on the basis of cubic pyrochlore structure with $Fd\bar{3}m$ symmetry.⁷ The selective strong and sharp peaks at C(222)

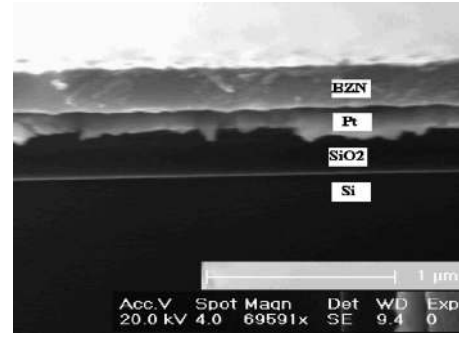


FIG. 2. Cross-sectional SEM of BZN thin film deposited at 650 °C. The measured thickness is 300 nm.

[“C” stands for cubic pyrochlore structure] indicate that the pulsed laser deposited films are highly textured. To look into the extent of preferred orientation, the orientation factors of the films have been calculated using Lotgering’s method.¹¹ According to Lotgering’s method, the degree of grain orientation f for BZN can be written as

$$f = \frac{p - p_0}{1 - p_0}, \quad (1)$$

where $p = \sum I_{222} / \sum I_{hkl}$ stands for the given oriented BZN thin films, and $p_0 = \sum I_{222} / \sum I_{hkl}$ for the BZN ceramic target. Here I_{hkl} and I_{222} are the intensities of the identified (hkl) and (222) peaks, respectively. It has been noticed that the BZN thin films are preferred C(222) oriented along with an orientation factor of 0.8. Moreover, it has been seen that there is a tendency of BiNbO_4 phase formation in bulk BZN, whereas such formations were not evident in the corresponding thin films. The pure phase formation of BZN excluding BiNbO_4 may be due to the combined effect of deposition parameters. The effect of deposition temperatures on crystallinity has been depicted in Fig. 1 with an inset of full-width half maxima (FWHM) of C(222) peaks with deposition temperatures. It has been observed that on increasing deposition temperatures, there is a constant fall of FWHM, which indicates the improving crystallinity with increasing deposition temperature. The recorded FWHM values for the temperatures of 500 °C, 550 °C, 600 °C, and 650 °C are 0.87, 0.69, 0.58, and 0.38, respectively.

Though the preferred orientation of BZN thin films indicates their anisotropic growth, a dense growth morphology of the films has been confirmed by the cross-sectional SEM micrograph (Fig. 2). The thickness of the film was also measured by the cross sectional SEM and the film thickness is confirmed to 300 nm. According to earlier reports,¹² the preparation of phase pure cubic pyrochlore BZN is difficult due to low sticking coefficients of Zn and Bi on substrate like platinized silicon and due to their high volatility. However, in the present study it has been seen that PLD grown BZN thin films at 650 °C is superior to its corresponding low temperature grown thin films by its better crystallinity maintaining the stoichiometry as well. Moreover, the diffraction refinements done by Levin *et al.*⁷ suggest that the large value of atomic temperature (displacement) parameters for both the O’ and (Bi/Zn) sites with the principal components

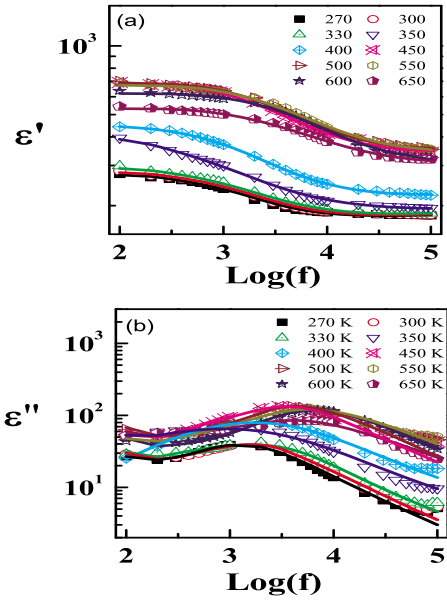


FIG. 3. (Color online) The frequency dependence of (a) ϵ' and (b) ϵ'' on a log-log scale at different temperatures. Scattered symbols: experimental data; solid lines: fitting to Eqs. (3) and (4).

perpendicular and parallel to the $\langle 111 \rangle$ can be responsible for the A site cation displacements confined to the $\{111\}$ or $\{222\}$ planes.

B. Dielectric response

The dielectric behavior in the pure cubic pyrochlore BZN thin films grown at 650 °C was investigated within a frequency region of 0.1–100 kHz and a temperature range of 270–650 K. The dielectric behavior of the films was presented in the form of frequency dispersion curves of the real (ϵ') and imaginary (ϵ'') parts of dielectric constants in Fig. 3. It has been observed that ϵ' exhibited the strong dielectric dispersion at low frequency ranging from 100 Hz to 10 kHz, whereas ϵ'' exhibited a strong dispersion throughout the frequency range with loss peaks shifting toward higher frequency region on increasing temperature. Moreover, ϵ'' exhibits a minimal dependence on frequency and lower temperature region and suggests the presence of a Maxwell–Wagner type of dielectric relaxation in the films.¹³ This phenomenon can also be supported by the step decrease in ϵ' at the frequency region of ϵ'' peaks. According to empirical Cole–Cole relation in Maxwell–Wagner type of dielectric relaxation, the complex dielectric constant can be represented as follows:^{13,14}

$$\epsilon^*(\omega) = \epsilon'(\omega) - i\epsilon''(\omega) = \left\{ \epsilon_\infty + \frac{(\epsilon_0 - \epsilon_\infty)}{[1 + (i\omega\tau)^\beta]} \right\} - i\frac{\sigma}{\omega}, \quad (2)$$

where ϵ_0 and ϵ_∞ are the static and high-frequency permittivity, respectively; σ is Ohmic conductivity, and τ is the most probable relaxation time or time constant. Here, β is a kind of numerical factor which indicates the distribution of relaxation times. The increment of β indicates the broader relaxation peak. The loss peak shifting toward higher frequency region on increasing temperature infers a Debye-type relaxation phenomenon and the factor β can be attributed to the

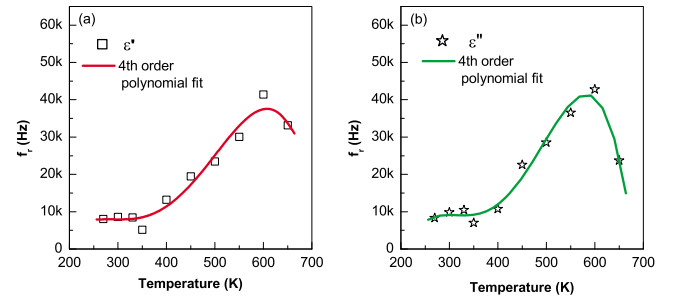


FIG. 4. (Color online) The relaxation frequencies, f_r on temperature obtained from equation fitting. In both the plots dielectric relaxation changes at 600 K indicating presence of two different relaxation process on temperature. The scattered dots are from fitted equation and solid lines are fourth order polynomial fitting as well as guide to the eyes.

broadening of the loss peak.¹³ The real and imaginary parts of $\epsilon^*(\omega)$ have been derived from the Eq. (2) giving their formulation as follows:

$$\epsilon' = \epsilon_\infty + \frac{\Delta\epsilon'}{2} \left\{ 1 - \frac{\sinh(\beta\varphi)}{\cosh(\beta\varphi) + \cos\left(\beta\frac{\pi}{2}\right)} \right\}, \quad (3)$$

$$\epsilon'' = \frac{\frac{\Delta\epsilon'}{2} \sin\left(\beta\frac{\pi}{2}\right)}{\cosh(\beta\varphi) + \cos\left(\beta\frac{\pi}{2}\right)} + \frac{\sigma}{\omega}, \quad (4)$$

where $\Delta\epsilon' = \epsilon_0 - \epsilon_\infty$ and $\varphi = \ln(\omega\tau)$.

In Fig. 3, the solid lines correspond to the fitting to Eqs. (3) and (4). From the fitted curve it has been found that the relaxation frequency (f_r), calculated from $\varphi = \ln(\omega\tau)$ and $f_r = 1/\tau$, increased with temperature up to 600 K for both the parts of dielectric constant (Fig. 4). Above the temperature the fall of relaxation frequency indicates the relaxation phenomena in the films changes above 600 K.

In Fig. 5 the real part of dielectric constant (ϵ') and dielectric loss factor ($\tan \delta$) are presented with respect to temperature at different frequencies. It has been seen that on increasing measurement temperature, there was a sudden rise in ϵ' . In addition, such rise in the threshold temperatures (T_{Th}) was also observed to depend on the frequency. The threshold temperatures seem to shift toward higher temperature region on increasing frequency, where the temperature of dielectric loss peaks (T_m) were also observed to follow the similar trend. To further gaining deeper understanding of dielectric relaxation, we have introduced the Arrhenius equations for both T_m and T_{Th} , and the expressions are presented as¹⁵

$$v = v_0 \exp\left[-\frac{E_a}{k_B T_m}\right], \quad (5)$$

$$f^l = f_0^l \exp\left[-\frac{E_b}{k_B T_{Th}}\right] \quad (6)$$

where v is the characteristic relaxation frequency, v_0 is attempt jump frequency, and E_a is the activation energy derived from the incremental of maximum dielectric loss peak

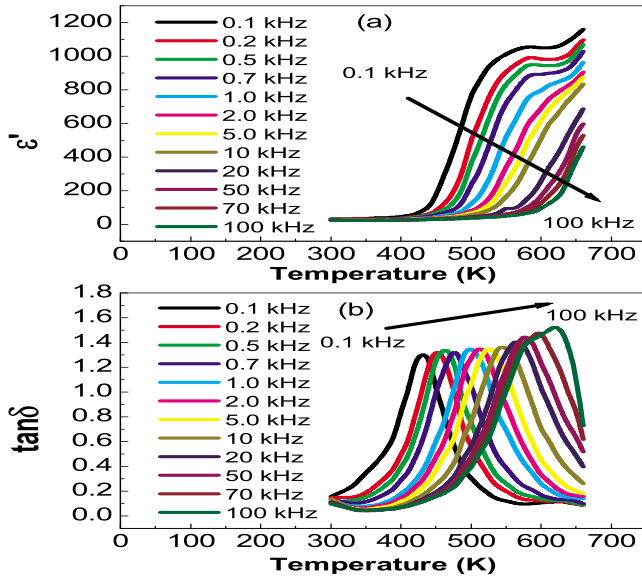


FIG. 5. (Color online) Temperature dependent real part of dielectric constant, ϵ' (a) and loss tangent, $\tan\delta$ (b). Changes in dielectric relaxations are obvious from the temperatures of maximum $\tan\delta$ peaks and threshold temperature of ϵ' at different frequencies.

temperatures (T_m). Similarly, f^1 is the characteristic relaxation frequency, f_0^1 is attempt jump frequency, and E_b is the activation energy derived from the incremental threshold temperatures (T_{Th}) of sudden rise in dielectric constants. From the logarithmic (Fig. 6), the calculated attempt jump frequencies are $\nu_0=2.2\times 10^{12}$ Hz and $f_0^1=2.1\times 10^{13}$ Hz. Though the attempt jump frequencies have the order of magnitude comparable to ionic vibrations in lattice, the differences observed between ν_0 and f_0^1 could be ascribed to the dc contribution in dielectric loss.⁹ The corresponding calculated activation energies are $E_a=0.9$ eV and $E_b=1.1$ eV.

As suggested in the Maxwell–Wagner type dielectric relaxation in BZN thin films, two kinds of dielectric relaxations are expected in their frequency dependent ac conductivity. To investigate the ac conductivity (σ_{ac}), studies were done with respect to frequency at different temperatures¹⁶

$$\sigma_{ac} = 2\pi f \epsilon_0 \epsilon' \tan\delta, \quad (7)$$

where f is frequency of conduction and ϵ_0 is the permittivity of vacuum. Though the trend of σ_{ac} in the frequency domain of 0.1–100 kHz [Fig. 7(a)] shows a conventional dependence on increasing temperature, the usual power law fails to keep its exponent n within 0 and 1. The conventional power law is read as¹⁷

$$\sigma_{ac} = \sigma_0 + A\omega^n, \quad (8)$$

where, σ_0 is frequency independent conductivity (commonly known as dc conductivity) and the coefficient A and exponent n are the temperature and materials intrinsic property dependent constants. Hence, the implementation of jump relaxation model appears to be appropriate and the existence of two different contributions to conductivity is validated. According to the jump relaxation model,¹⁸ the successful ion hops to its neighborhood vacant site due to the available long time period contributes to the conductivity in low frequency region, and such successive jumps result in a long transla-

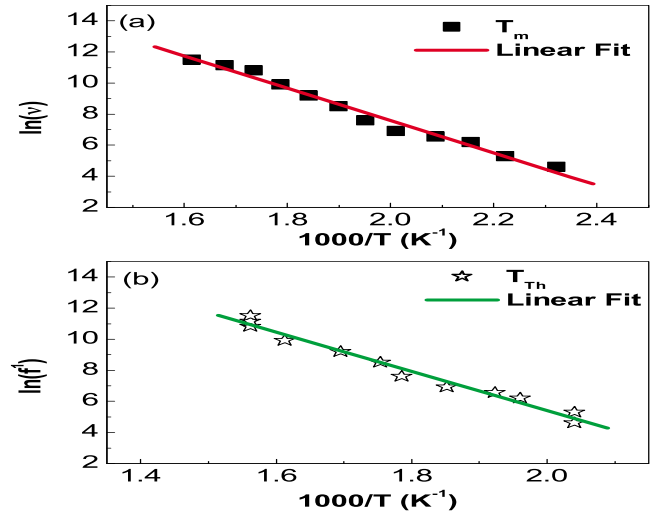


FIG. 6. (Color online) The frequency dependent Arrhenius plots of maximum temperatures (T_m) of $\tan\delta$ (a) and threshold temperatures (T_{Th}) of ϵ' (b). Attempt jump frequency for $\tan\delta$, $\nu_0=2.2\times 10^{12}$ Hz and attempt jump frequency for ϵ' , $f_0^1=2.1\times 10^{13}$ Hz.

tional motion. Since two different kinds of relaxations can be visualized at higher frequencies such as; (i) correlated ion position related to back and forth jumping, i.e., unsuccessful hopping and (ii) once jumped ions become relaxed and stay in the new site, i.e., successful hopping. As the ratio of successful to unsuccessful hopping increases, the dispersive conductivity at high frequency is observed. Assuming the jump relaxation model playing role into the BZN, the σ_{ac} conductivity data has been fitted to a double power law^{17,18}

$$\sigma_{ac} = \sigma_0 + A_1\omega^{n_1} + A_2\omega^{n_2}, \quad (9)$$

to describe a two different contributions to σ_{ac} . From the fitted data [presented in Fig. 7(a), solid lines] it has been seen that in the lower frequency region, the exponent $0 < n_1 < 1$ indicates the translational hopping motion (short range hopping). In the high frequency region, the exponent with the values ranging as: $0 < n_2 < 2$ (characterize the localized or reorientational hopping motion), the absence of frequency independent part within the frequency window (0.1–100 kHz) excludes the response of translational hopping for long range electrical transport and could be one of the expected reasons for dc conductivity. From Fig. 7(b), it can be seen that there is a steady decrease in n_1 values with increasing temperature, which indicates that the exponent at low frequency region is due to large polaron hopping. It is known that the polaronic hopping with large energy barriers contributes to ac conductivity. At higher temperatures there are two peaks observed in n_2 values which indicates that in the high frequency region, a cross over from grain to grain boundary is existent. It is well known from the earlier report¹⁷ that small polaronic hopping is ascribed to an increment of exponent values with increasing temperature while the large polaronic hopping causes decrease in exponent values. From the trend of n_2 values with temperature, it can be predicted that in low temperature region, the true response of grains is exhibited at high frequency region which has been obscured by the large polaronic hopping with increasing temperature. Hence decrease in n_2 value was observed. However, at the

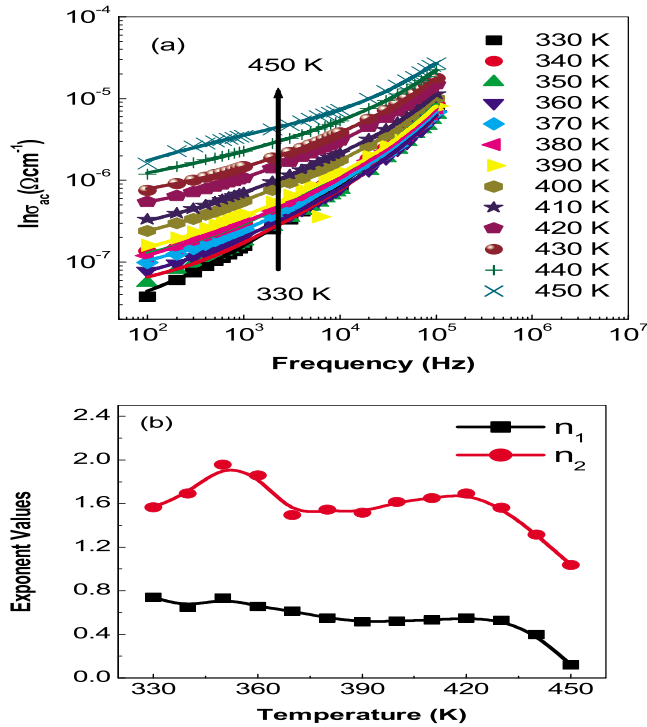


FIG. 7. (Color online) ac conductivity of BZN thin films at various temperatures plotted against frequency (a). On increasing temperature there is an increase in conductivity and change in nature are obvious. (b) The power exponents due jump relaxation model; n_1 : low frequency exponent and n_2 : high frequency exponent.

onset of crossover from grains to grain boundary, the small polaronic hopping in grain boundaries again dominates the exponents on increasing temperature giving rise a second peak at 420 K. The activation energy of long range polaronic hopping has been quantified by ac conductivity based Arrhenius plot in Fig. 8. The corresponding equation of Arrhenius plots is read as

$$\sigma_{ac} = \sigma' \exp(-E_a/kT), \quad (10)$$

where σ' is the pre-exponential factor of conductivity, E_a is the activation energy of ac conductivity, k is the Boltzmann constant, and T is temperature in absolute scale. It has been seen that there are two different regions of activation energies associated to polaronic hopping. It has been noticed that

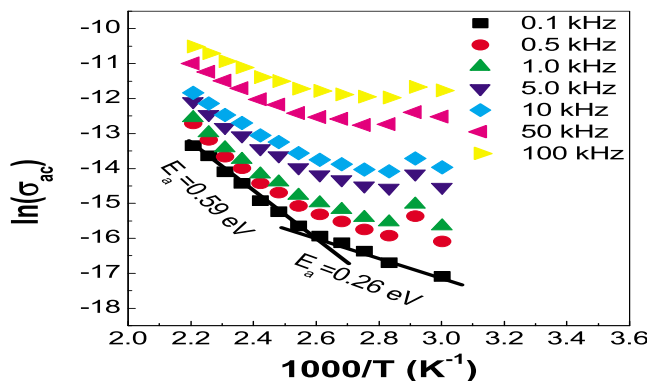


FIG. 8. (Color online) Arrhenius plots at different frequencies from temperature dependent ac conductivity. At 0.1 kHz low temperature activation energy of polaronic hopping is 0.26 and 0.59 eV is for high temperature.

polaronic hopping, corresponding to 0.26 eV activation energy (E_a), is mostly attributed to low temperature region at 100 Hz, whereas the polaronic hopping at high activation energy ($E_a=0.59$ eV) responses at high temperature region. From the Arrhenius plots, it has been observed that with increasing frequency, the slopes of the curves or the activation energies of the polaronic hopping response are decreasing, manifesting a small polaronic hopping at higher frequencies. However, the kinks at higher frequencies in Arrhenius plots again suggest a grain to grain boundary transition in ac conductivity (exhibited at high frequency region and associated with small polaronic hopping). Moreover, the range of activation energies in the low frequency region (0.26–0.59 eV) can be understand in terms of commonly present oxygen vacancies in oxide thin films.¹⁶

To investigate the two kind of dielectric response, Nyquist plots¹³ have been studied at different temperature (Fig. 9). It has been observed that up to 450 K there was no indication of different response contributions. Though the ac conductivity shows a phase transition at 420 K, the Nyquist plot shows such transition at 450 K. Such deviation may be due to the interference of internal induction effect contributed to impedance. However, the suspected transition from grain to grain boundary presumes that in the low temperature region, BZN thin films exhibit possibly true grain dependent characteristics, whereas the transitions at 480 K, 540 and 600 K reveals clear grain boundary contribution.

To look into the grain boundary and grain contributions in BZN thin films, as there is always a question of special kind of crystal structure of BZN, the concept of grain and grain boundary contribution should be critically evaluated. From the Arrhenius plots in Fig. 6(a) shows that there is a steady phase transition in $\tan \delta$ up to 620 K which corresponds to the attempt jump frequency ($\nu_0=2.2 \times 10^{12}$) which in at the range of BZN's lattice vibronic mode.⁹ It is well known from the earlier reports⁷ that the polaronic hopping in C-BZN is related to abnormally large values of atomic temperature (displacement) parameters for both the O' and (Bi/Zn) sites and to some extent large O atom (48f sites) displacements consistent with local tilting of $[(\text{Nb}, \text{Zn})\text{O}_6]$ octahedral. Thus, it can be interpreted that the grain and grain boundarylike response can be attributed to temperature dependent different anisotropy in the films. This tentative observation can explain both the attempt jump frequency in BZN thin films as well as the two different dielectric responses. Since, an appreciable distortion of the A-site with the principal components of displacement directed perpendicular and parallel to the $\langle 111 \rangle$ directions, it is suggested that A-site displacement is confined in $\{111\}$. Thus the preferred C(222) orientation of BZN thin films suggests that the temperature dependent different anisotropy is mostly due to A-site rattling. Thus small polaronic hopping as well as long polaronic hopping can be expected within the crystal structure depending on the temperature dependent distortion and anisotropy in BZN thin films. Hence the polaronic phase transitions studied in the present work through the jump relaxation exponent in high temperatures, high frequency region, can be attributed to BZN's intrinsic properties rather than defect induced polaronic hopping at lower frequencies.

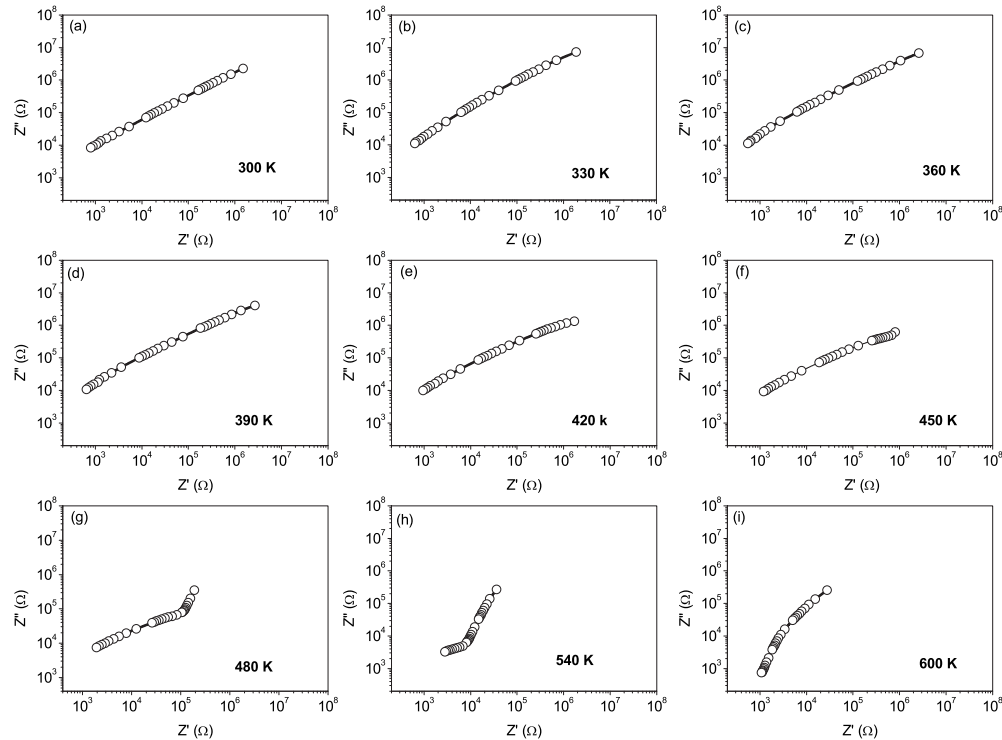


FIG. 9. Temperature dependent Nyquist plots at various temperatures. The crossover from one kind of impedance response to another kind is distinguished from the presentations of 450, 480, 540, and 600 K.

This phenomenon is supported by the presence of high temperature dielectric loss maxima as well as threshold temperature of real part of dielectric constant and their corresponding attempt jump frequencies in the range of lattice vibronic mode.

IV. CONCLUSIONS

Cubic pyrochlore BZN thin films have been prepared on Pt(200)/SiO₂/Si substrates by PLD with a preferred orientation of C(222). The dielectric properties of BZN thin films within the frequency range of 0.1–100 kHz and temperature range of 270–650 K shows a Maxwell–Wagner type response. Though the jump relaxation model suggested that there is an interference of grain boundaries at high frequencies, the calculated attempt jump frequencies in the range of lattice vibronic frequencies excludes the possibilities. Moreover, it is suggested that in the high frequency region the existence of small and long polaronic hopping in BZN can be speculated with increasing temperature due its structural anomaly and structural distortion. The attempt jump frequency has been calculated in the range of 10¹²–10¹³ Hz whereas at low frequency, calculated activation energy of polaronic hopping found to vary from 0.29 to 0.59 eV with increasing temperature.

- ¹J. W. Lu and S. Stemmer, *Appl. Phys. Lett.* **83**, 2411 (2003).
- ²J. Park, J. W. Lu, S. Stemmer, and R. A. York, *J. Appl. Phys.* **97**, 084110 (2005).
- ³J. W. Lu, Z. Q. Chen, T. R. Taylor, and S. Stemmer, *J. Vac. Sci. Technol. A* **21**, 1745 (2003).
- ⁴S. W. Jiang, B. Jiang, X. Z. Liu, and Y. R. Li, *J. Vac. Sci. Technol. A* **24**, 261 (2006).
- ⁵X. Wang, H. Wang, and X. Yao, *J. Am. Ceram. Soc.* **80**, 2745 (1997).
- ⁶J. C. Nino, M. T. Lanagan, and C. A. Randall, *J. Appl. Phys.* **89**, 4512 (2001).
- ⁷I. Levin, T. G. Amos, J. C. Nino, T. A. Vanderah, C. A. Randall, and M. T. Lanagan, *J. Solid State Chem.* **168**, 69 (2002).
- ⁸I. Levin, T. G. Amos, J. C. Nino, T. A. Vanderah, I. M. Reaney, C. A. Randall, and M. T. Lanagan, *J. Mater. Res.* **17**, 1406 (2002).
- ⁹S. Kamba, V. Prokhonsky, V. Bovtun, A. Pashkin, J. Petzelt, J. C. Nino, S. Trollet-McKinstry, M. T. Lanagan, and C. A. Randall, *Phys. Rev. B* **66**, 054106 (2002).
- ¹⁰M. A. Subramanian, G. Aravamudan, and G. V. Subba Rao, *Prog. Solid State Chem.* **15**, 55 (1983).
- ¹¹F. K. Lotgering, *J. Inorg. Nucl. Chem.* **9**, 113 (1959).
- ¹²J. Lu, D. O. Klenov, and S. Stemmer, *Appl. Phys. Lett.* **84**, 957 (2004).
- ¹³J. Liu, C.-G. Duan, W.-G. Yin, W. N. Mei, R. W. Smith, and J. R. Hardy, *Phys. Rev. B* **70**, 144106 (2004).
- ¹⁴A. K. Jonscher, *Dielectric Relaxation in Solids* (Chelsea Dielectric, London, 1983).
- ¹⁵C. Ang, Z. Yu, H. J. Youn, C. A. Randall, A. S. Bhalla, L. E. Cross, J. Nino, and M. Lanagan, *Appl. Phys. Lett.* **80**, 4807 (2002).
- ¹⁶S. Bhattacharyya, S. S. N. Bharadwaja, and S. B. Krupanidhi, *J. Appl. Phys.* **88**, 4294 (2000).
- ¹⁷N. Ortega, A. Kumar, P. Bhattacharya, S. B. Majumder, and R. S. Katiyar, *Phys. Rev. B* **77**, 014111 (2008).
- ¹⁸K. Funke, *Prog. Solid State Chem.* **22**, 111 (1993).

Journal of Applied Physics is copyrighted by the American Institute of Physics (AIP). Redistribution of journal material is subject to the AIP online journal license and/or AIP copyright. For more information, see <http://ojps.aip.org/japo/japcr/jsp>